Open Ceramics 9 (2022) 100232

Contents lists available at ScienceDirect

Open Ceramics

journal homepage: www.sciencedirect.com/journal/open-ceramics

Red firing clays for the manufacture of vessels for wine fermentation and maturation by means of technological processes

Francisca Quereda Vázquez [a], M-Magdalena Lorente-Ayza [a,*], Nevares Ignacio [b], del Alamo-Sanza María [c], Pamela Escrig Marín [a], María Ojeda Doménech [a]

[a] Instituto de Tecnología Cerámica (ITC), Asociación de Investigación de las Industrias Cerámicas (AICE), Campus Universitario Riu Sec, Av. Vicent Sos Baynat s/n, 12006, Castellón, Spain
[b] Department of Agricultural and Forestry Engineering, UVaMOX, Universidad de Valladolid, Unidad Asociada al CSIC, 34004, Palencia, Spain
[c] Department of Analytical Chemistry, UVaMOX, Universidad de Valladolid, Unidad Asociada al CSIC, 34004, Palencia, Spain

ARTICLE INFO

Keywords:
Ceramic vessel
Red firing clays
Pore size distribution
Permeability
Oxygen transmission rate
Firing behavior

ABSTRACT

Different red firing clays (Teruel, Villar and Yesa) from the Iberian orographic system of Spain (Castellón/Teruel/Valencia) have been studied to analyze their suitability for the manufacture of technology-based ceramic vessels, studying their characterization from a ceramic technical perspective (open porosity, permeability, pore size, microstructure, process behavior, etc.), as well as from a wine maker perspective (oxygen transmission rate, *OTR*). The three clays have been proved as suitable for the manufacture of ceramic vessels because of their adequate behavior in the manufacturing process (although Yesa clay provides higher proneness to deform by pyroplasticity at high firing temperatures, that is, low porosities) and similar permeability with respect to certain types of existing ceramic vessels. Compared to available data of *OTR*, the values obtained are lower but with the same order of magnitude, and other clays from the same region have been postulated as the key for achieving higher *OTRs*.

1. Introduction

Traditionally, earthenware vessels were used in the past for the elaboration and conservation of wine and, on some occasions, for its fermentation. However, in the mid-20th century, other materials began to be used in the winemaking process, such as concrete, stainless steel or wood.

Currently, some wineries and winemakers are recovering old ceramic vessels for the production of differentiated wines, due to the properties that ceramics provide. Others are using newly made earthenware vessels, manufactured by artisanal processes, for the vinification of their grapes. However, both old and handmade earthenware vessels have very different characteristics, due to the variety of materials used (usually of local origin) and the manufacturing process (manual and discontinuous). This affects to the characteristics of the wine obtained, since parameters such as the dimensions of the vessel, its composition, porosity and pore size distribution influence the fermentation and maturation process.

Ancient vessels were made of earthenware or clay and they were fired at a low temperature (700-1080 °C) in oxidant atmospheres. They were red, yellow or white, depending on the geographical origin, and they were traditionally very porous, so many of them were permeable to wine and had to be waterproofed in their inner surface with beeswax or other sealing substances to avoid wine leaks [1,2].

Modern ceramic vessels can be produced at higher temperatures (above 1200 °C), obtaining relatively dense materials, in contrast to the characteristically porous earthenware, with reduced porosity, which can provide oxygen transport without contributing any tannins or coloration, in contrast to oak barrels [3]. Moreover, as they have reduced porosity, no internal sealing is needed.

Most of the ceramic vessels produced nowadays in Spain are handcrafted, obtaining products with different characteristics, especially regarding microstructure and porosity. Moreover, owed to their high porosity, many of them should be covered with waterproof materials in their inside to avoid filtration, following the same procedure than with ancient jars. Examples of this kind of vessels are those manufactured by Tinajas Orozco [31] and Tinajas Moreno León [32], located in Spain, both manufactured manually and sintered in wood ovens at lower

* Corresponding author. Asociación de Investigación de las Industrias Cerámicas, Instituto de Tecnología Cerámica, Campus Universitario Riu Sec, Av. Vicent Sos Baynat s/n, 12006, Castellón, Spain.
E-mail address: magda.lorente@itc.uji.es (M.-M. Lorente-Ayza).

https://doi.org/10.1016/j.oceram.2022.100232
Received 30 November 2021; Received in revised form 18 January 2022; Accepted 9 February 2022
Available online 17 February 2022

temperatures. Other manufacturer is the Swiss company Oeno-Tech [33], which produces stoneware vessels, handmade and sintered at 1300 °C. In addition, Tava [34], Italian company, also produces artisanal ceramic vessels at temperatures between 1200 and 1260 °C with controlled porosity. Nevertheless, none of these companies give data about the porosity and microstructure of their products, in many cases lacking of reproducibility in their properties.

Related to ceramic vessels industrially manufactured, there are two producers in the European Union: Biopythos [35] in France and Clayver [36] in Italy. Biopythos produces stoneware and porcelain vessels by traditional casting, which differ in their composition and permeability: stoneware is made from ¼ clay, ¼ kaolin, ¼ feldspar and ¼ silica (61.5% SiO_2; 33.9% Al_2O_3; 1.7% K_2O) while porcelain is formulated from ½ kaolin, ¼ feldspar and ¼ silica (68.9% SiO_2; 26.1% Al_2O_3; 3.4% K_2O). The only microstructural characterization given of both compositions is porosity, being porcelain less micro-oxygenating (2%) than stoneware. According to Clayver web page, their ceramic wine vessels are made of a particular homogeneous and compact natural ceramic stoneware, which is impermeable to liquids and therefore it does not need any sealing in order to avoid evaporation; the intrinsic microporous structure of the ceramic material can allow a gaseous exchange with the outside of the container but only in limited quantities and on very long time scales, being made by plastic pressing and firing around 1200 °C [1,4]. The most relevant properties of this material are: bulk density 2.34 g/cm^3, water absorption 2.1% (porosity of 5%), average pore diameter 0.04 μm, permeability $4.6 \cdot 10^{-18}$ m^2, flow O_2 standard type 5 mg/L/year and type O^+ 13 mg/L/year.

Finally, Alfatec Ingeniería y Consultoría carried out the Dolia Project in 2014, developing ceramic technological barrels made of different clays and analyzing the oxygen flow of different samples and comparing them with ancient jars and with oak barrels [4].

Table 1 sums up the main properties of the different ceramic vessels referred in the literature and from authors' research and compares these data with oak barrel properties. As it can be seen, few information about the characteristics of vessels and their compositions are given.

One of the objectives of the project "GOVALMAVIN. Valorization of traditional materials for the vinification of quality wines" is the development of an automated manufacturing process, which, together with the selection of the raw materials used, guarantees the manufacture of technology-based ceramic vessels, whose properties are homogeneous and reproducible. In this way, it will be possible to guarantee that the effect of the vessel on the evolution and properties of the wine will be known and controllable.

Fig. 1 shows the conventional manufacturing processes for ceramic products. Regardless of the type of ceramic product, the following stages can be distinguished: preparation of the composition, shaping, drying and firing. There is a direct relationship between the composition preparation processes and the type of shaping of the piece, given that each shaping process requires different characteristics in terms of both water content (necessary for shaping) and particle size of the raw materials mixture.

In the case of vessels, given their geometry, the most suitable technological processes are casting and plastic shaping: extrusion + pressing/turning/3D printing. In the case of casting, only Biopythos [35] in France, as already stated, has been found to use this process, but no company has been identified in Spain that could implement this manufacturing process. On the contrary, it is considered more feasible to design a process similar to that of ceramic roof tiles or porcelain insulators together. The third option would be additive manufacturing, which would allow the workpiece to be made as a whole from the extruded mass [37]. This third option is a promising process which was used very recently for the manufacture of a small quantity of vessels but there are no companies in Spain capable of manufacturing vessels with this technology.

Therefore, the most efficient process for the industrial manufacture of ceramic vessels in Spain is that consisting of the dry milling of the raw materials with a pendulum mill (since in this way it is possible to obtain distributions of small particle size and, therefore, vessels with small pore sizes), followed by kneading and shaping of the mixture of raw materials by extrusion. The different parts of the vessel should then be shaped by plastic pressing, wet-welded together (welding would be done with a suspension obtained from the same ceramic composition, process already used in the manufacture of ceramic sanitary ware and tableware) and then dried and fired. Critical in this process is the water content suitable for the shaping process, which depends on the clays used. This water content must be as low as possible, but ensuring the workability of the material, so that the drying shrinkage could be as low as possible and the rigidness of material to be sufficiently high after shaping to avoid deformation.

Regarding raw materials, different options can be found, ranging from Spanish red firing clays used in the manufacture of ceramic stoneware tiles to compositions of tableware porcelain (mixture of ball clays, kaolin, feldspar and quartz) if they are ordered taking into account firing temperature. The lowest firing temperature being around 1100 °C (ceramic tiles) and the highest around 1400 °C (tableware porcelain). Intermediate compositions would be for instance those used in sanitaryware, with firing temperatures around 1250 °C. All these compositions exhibit an adequate firing behavior in terms of shrinkage and pyroplastic deformation at their optimum firing conditions. From a Life Cycle perspective, the lowest impact would be the use of local red firing clays as the distance of transport of these clays to the ceramic producer would be low and energy consumption of the manufacturing process would also be low.

For this reason, in this paper, different red clays from the Iberian orographic system of Spain (Castellón/Teruel/Valencia) have been studied to analyze their suitability for the manufacture of technology-based ceramic vessels, studying their characterization from a ceramic technical perspective (open porosity, permeability, pore size, microstructure, process behavior, etc.), as well as from a wine maker perspective (oxygen transmission rate).

2. Material and methods

In the present work, three different clays from the Iberian orographic system of Spain (Castellón/Teruel/Valencia) were analyzed: Villar, Yesa and Teruel. All these raw materials are used in the manufacturing of red firing ceramic stoneware tiles in Spain.

Villar and Yesa type clays can be found in the Lower Cretaceous-Upper Jurassic strata, in the Utrillas and Wealdiense facies. The most important deposits are located between the towns of Villar del

Table 1
Summary of the main properties of vessels (data from the literature and from authors' research) (T: firing temperature, ε: porosity, d_p: pore size, K_p: permeability).

Origin	Composition	T (°C)	ε (%)	d_p (μm)	$K_p \cdot 10^{18}$ (m^2)	flow O_2 (mg/liter/year)	Ref.
Ancient ceramic jars	earthenware/clay	700–1080	22–29	–	–	44	[1,2,4]
Biopythos	stoneware	–	>2	–	–	–	[35]
	porcelain	–	2	–	–	–	
Clayver	stoneware	1200	5	0.04	4.6	5	[1,36]
Dolia 2	clay	1310	16	0.57	25	17	[4]
Dolia 5	clay	1000–1050	3–8	0.10–0.12	0.1–0.4	8	[4]

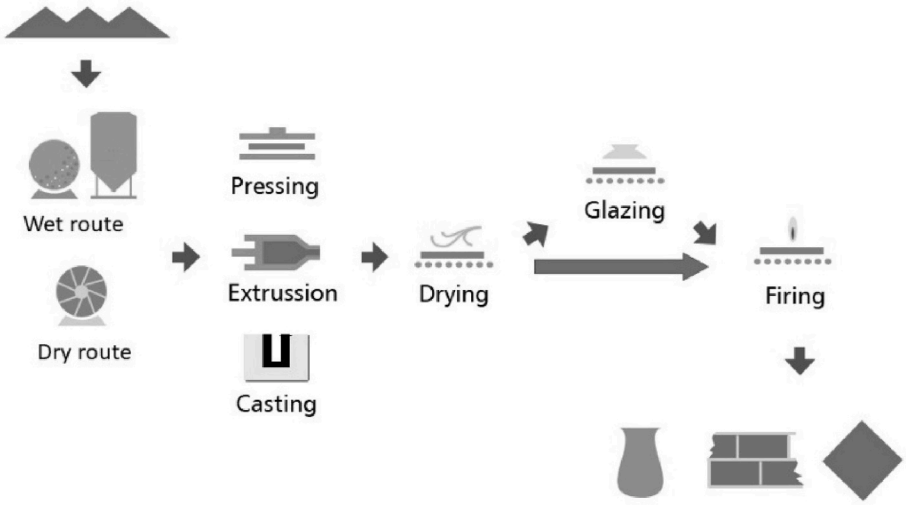

Fig. 1. Conventional manufacturing processes for ceramic products.

Arzobispo, Higueruelas, Andilla and La Yesa (Spain). The area is geologically complicated, with abundant faults, so the deposits do not have a great continuity. These are normally of limited capacity, with interbedded layers of kaoliniferous sands of the Wealdiense facies. In addition, calcareous layers and nodules, coal and pyrite may appear as impurities, the presence of the latter two being infrequent. Villar clay corresponds to the deposits of Villar del Arzobispo and Yesa to the deposit of the equally named town, both in the province of Valencia. These two clays are illitic-kaolinitic, varying their kaolinitic character and quartz content depending on the area of exploitation and, therefore, their plasticity and behavior during firing [5,6].

Teruel clay has been obtained from the deposit of Mora de Rubielos (Teruel, Spain) in the Galve Sub-basin (Maestrazgo basin). The clay belongs to the Camarillas Formation of the Wealdiense facies which in this region contains abundant deposits of kaolinitic clays. The Maestrazgo basin was generated between the end of the Jurassic period and the beginning of the Cretaceous period, same period of origin of Villar and Yesa clays. The Maestrazgo basin consists of a system of extensional basins, generally highly subsiding, which will remain until the Upper Cretaceous in the whole Iberian Basin [7].

The samples used in this study have been taken from homogenized stocks of the three clays already used by ceramic tile producers in order to reduce typical variability of mineralogy and properties of these types of clays. Table 2 displays the chemical and mineralogical composition of the clays.

Table 2
Chemical and mineralogical compositions of the raw materials used (wt %).

	Villar	Yesa	Teruel
SiO_2	62	60	59
Al_2O_3	18	22	25
Fe_2O_3	6.3	6.2	7.0
CaO	1.5	0.5	0.2
MgO	1.3	0.3	0.3
Na_2O	0.4	0.3	0.1
K_2O	4.0	4.9	1.2
TiO_2	1.1	1.1	1.2
Loss on ignition	5.7	5.1	6.8
Quartz	37	35	29
Illite/M. Muskovite	22	35	8
Kaolinite	19	10	55
Feldspar	8	5	–
Calcite	3	1	1
Hematite	6	6	7
Others	5	8	–

The clays were dry milled in a pendulum mill. The particle size distribution of the milled clays was obtained by X-ray absorption-controlled sedimentation. The clay sample was dispersed in an aqueous solution of 1.8 g of sodium hexametaphosphate and 0.4 g of anhydrous sodium carbonate in 1 L of water. It was then subjected to ultrasounds for 5 min and left to stand for at least 24 h in order to achieve complete dispersion of the particles. After this time, it was again subjected to 5 min of ultrasounds and magnetic stirring before being placed in the cuvette of the apparatus for measurement. The equipment used to carry out the particle size analysis was a MICROMERITICS SEDIGRAPH 5120. The test was carried out considering a density of 2.63 g/cm^3 for the clays and sieving the samples previously with a 63-μm sieve.

The reject on 63-μm sieve was obtained by following the same preparation procedure as the suspensions to be analyzed in the equipment, before passing them through the corresponding sieve.

The plasticity index was calculated by the indentation method [8–10]. This method consists of determining the force required to introduce an indenter with a conical end into masses prepared at different moisture contents. The value of the force when the cone is entirely introduced is considered to be the consistency value of the mass at that moisture content. When the consistency is plotted on logarithmic coordinates versus moisture content, a straight line is obtained from which the moisture contents corresponding to the Atterberg limits (liquid and plastic limit) are determined. Plasticity index is then calculated as the difference between the liquid limit and the plastic limit.

Each clay was kneaded with the amount of water corresponding to the plastic limit with an extra 1 wt% to ensure an adequate flow in the extruder (water content close to plastic limit is typical in extrusion of ceramic compositions such as extruded tiles, rooftiles, tableware porcelain and porcelain insulators) and allowed to stand for 24 h to achieve uniform moisture in the mass. Test pieces 1 cm thick and 10 cm wide were extruded, using a laboratory auger with a de-airing chamber (Model 050C, Talleres Felipe Verdés, S.A., Spain). The test samples were weighed and afterwards dried at room temperature for 24 h, and oven-dried at 110 °C to a constant weight.

After drying, all the samples were weighed, and the bulk density was measured by the Archimedes displacement technique using mercury as non-wetting liquid [11]. Next, the dried specimens were then sintered in an electric laboratory kiln with a thermal cycle characterized by a heating speed of 5 °C/min and a soaking time of 60 min at different maximum temperatures (between 950 and 1200 °C).

After firing, the samples properties were determined. These properties included density (measured by the mercury displacement method),

linear shrinkage, water absorption (boiling water immersion method [5]) and porosity.

Pyroplastic deformation was also measured [12,13]. For this test, prismatic test pieces (80 mm long, 20 mm wide, and about 7 mm thick) were cut from the extruded and dried specimens. In order to perform the firing, the test pieces rested only on their two ends, so that they were able to deform during firing. Finally, the proneness to deform by pyroplasticity was evaluated, the pyroplasticity index (*PI*) being calculated from the following expression:

$$PI = \frac{4 \cdot e^2 \cdot s}{3 \cdot L^4} \tag{1}$$

where e is the thickness of the piece, s the measured sag and L the distance between supports.

The pore size distribution was measured by mercury intrusion porosimetry (AutoPore IV 9500, Micromeritics Instruments Co, USA), and the total volume of pores (Vt) and characteristic pore diameters (d_{16}, d_{50}, and d_{84}), were calculated.

To study the sample microstructures, polished specimen cross-sections were observed by optical microscopy (Olympus BX-60).

Air permeability was calculated by measuring the air flow through the sample at room temperature in a special device (Fig. 2). To carry out the test, a cylindrical specimen cut from the fired pieces, the side surface of which has been previously sealed to prevent air loss through it, is placed in the permeability cell as shown in Fig. 2. By suitably modifying the pressure regulating valve, a pressure gradient across the specimen is set on the manometer. Then, for each value of the pressure gradient, the time taken for a perfectly measured volume of air to flow through the specimen is determined with the flowmeter. At least five different pressure gradients are determined for each specimen. Air permeability K_p (m^2) is calculated from the equation:

$$K_p = \frac{2 \cdot \mu_a \cdot Q_a \cdot L}{S} \cdot \frac{P_{atm}}{(P_1^2 - P_2^2)} \tag{2}$$

where μ_a is the air viscosity at room temperature ($N \cdot s/m^2$), Q_a is the air flow rate (m^3/s), L is the specimen thickness (m), S is the air cross section (m^2), P_{atm} is the atmospheric pressure (N/m^2), P_1 is ($P_{atm} + \Delta P$) (N/m^2), ΔP is the stablished gradient pressure (N/m^2) and P_2 is P_{atm}.

Oxygen permeation can be measured using the total pressure method, as in the air permeability measurement previously described, being the total pressure the driving force under Darcy's law. There are other two ways, the isostatic and quasi-isostatic methods [14]. The isostatic methods establish a difference between the partial pressure of oxygen on both sides of the material to be characterized, while the total pressure on both sides of the material remains similar. In the quasi-isostatic method, the coefficient of permeability needs to be measured to have a permanent gas transfer, which is achieved when equal amounts of O_2 enter and leave the barrier material. In the first stage of the permeability process, the solubility of atmospheric O_2 in the barrier material is dominant. As the concentration gradient increases on both sides of the material, the second stage of O_2 diffusion becomes the main contributor to O_2 permeation [15].

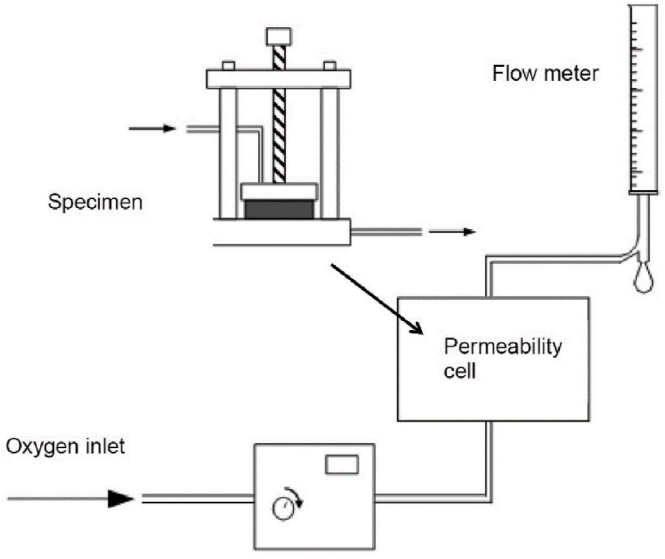

Fig. 2. Assembly used for the determination of oxygen permeability.

Measuring permeation as a flux of molecules (permeant) through a material, when there is equal static pressure on both sides of the barrier, but the partial pressure of the permeant gas is different, is governed by the Fick's first law of diffusion [Eq. (3)], and is the process called diffusion, movement of molecules as a result of random molecular motion when the driving force is the concentration gradient.

$$J = -D \cdot \frac{\delta c}{\delta x} \tag{3}$$

The permeation coefficient (permeability) P ($m^3(STP) \cdot m/m^2 \cdot s \cdot Pa$) is the product of the diffusion coefficient (diffusivity) D (m^2/s), and Henry's law solubility coefficient (solubility) S ($m^3(STP)/m^3 \cdot Pa$) of the gas in the membrane [Eq. (4)], which is the ratio between its concentration c (m^3 $(STP)/m^3$) in the membrane and its partial pressure p (1/Pa) in the gas phase at a constant temperature [14,16,17] [Eq. (5)].

$$P = D \cdot S \tag{4}$$

$$S = \frac{c}{p} \tag{5}$$

The flow of O_2 gas J transported per unit of time through the surface of a membrane, also known as Oxygen Transmission Rate (*OTR*) and the commonly used unit of (cm^3 $(STP)/m^2 \cdot day$), is proportional to the constant partial pressure gradient Δp (Pa) between both sides of the membrane (p_{atm} and p_0) of thickness L (m) [Eq. (6)] [18].

$$OTR = D \cdot S \cdot \frac{\Delta p}{L} = P \cdot \frac{p_{atm} - p_0}{L} \tag{6}$$

The Time lag method record the variation of the oxygen partial pressure in the permeation cell measurement chamber at constant volume and constant total pressure and describes how to determine the time needed to obtain steady-state permeability of a gas—taking into account the contribution of diffusion and sorption to overall permeability (Fig. 3). The measurement of the oxygen partial pressure p_{O2} was performed with an optoluminescent Fibox 4 Trace meter and a sensor probe PSt6 (PreSens GmbH, Germany, limit of detection 0.002% oxygen) calibrated before each test, connected to a PC and controlled with the software PreSens Measurement Studio 2 version 3.0.3 (PreSens GmbH, Germany). In addition, an infiltration test of the measurement chamber was performed to determine the base infiltration that was subsequently subtracted from the measurement.

The outflow time lag, θ_L, is obtained by extrapolating the asymptote of the linear steady-state portion of the pressure profile to the time axis (Fig. 3) [19]. In turn, the diffusion coefficient is inversely proportional to the time lag [Eq. (7)],

$$D = \frac{L^2}{6\,\theta_L} \tag{7}$$

OTR in the steady-state region is calculated from the slope of the increment of the p_{O2} over time, the volume of the measurement chamber V and the surface of the measured membrane A considering atmospheric pressure p_{atm} [20] [Eq. (8)],

$$OTR = \frac{\Delta p_{O2}}{\Delta t} \cdot \frac{V}{A \cdot p_{atm}} \tag{8}$$

The permeation coefficient [Eq. (9)] is obtained from Eq. (6), which

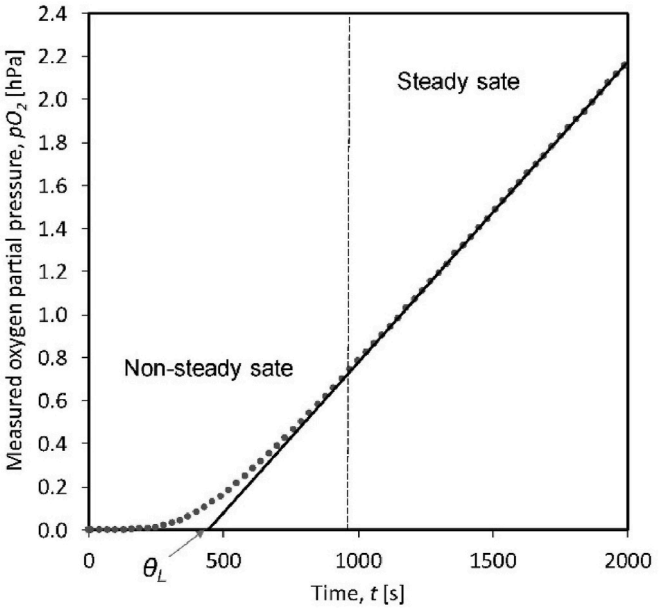

Fig. 3. A plot of oxygen partial increment versus time in the oxygen-free chamber.

also allows the S to be determined thanks to Eq. (4).

$$P = OTR \cdot \frac{L}{p_{atm} - p_0} \tag{9}$$

Time Lag Test Setup and Procedure. Before the start of the test, the samples were subjected to successive vacuum phases by means of an RZ-6 pump with CVC-3000 controller (Vacuubrand GmbH, Germany) connecting both chambers located on both sides of the sample under study. The vacuum level reached during the vacuum phases was 10^{-3} mbar measured with a sensor based on thermal conductivity (Pirani) VSP-3000 (Vacuubrand GmbH, Germany). Four vacuum cycles were carried out and the corresponding balance with the inert gas, to ensure the emptying of the atmospheric O_2 from the interior of the material's porosity. The first vacuum phase lasted 24 h and an inert gas, in our case N_2 (Carburos Metálicos/Airproducts, Spain), was used to equilibrate the pressure in both chambers with the surrounding atmospheric pressure. The following vacuum cycles were of 1h with the corresponding N_2 balance. Once the vacuum cycles were finished and the balance with the inert gas was done, it was checked that the sample ceramics did not contain air inside them by measuring the increase of the partial pressure of O_2 for 1 h. The test was then started by leaving one side of the ceramic sample opposite the measurement chamber of the material in contact with the atmospheric air (Fig. 4).

All ceramic samples were measured in triplicate and the tests were carried out under controlled temperature and RH conditions (14 °C and 75% RH).

3. Results

3.1. Behavior of the clays in the manufacturing process

The characterization of the three clays aimed at determining their behavior in the proposed manufacturing process of the vessels (dry milling, extrusion, plastic shaping and firing) as well as their influence on the key properties regarding their intended use in wine making (porosity, air permeability and oxygen transfer rate). In this section the properties related to their behavior in the manufacturing process as well as intrinsic ones are evaluated and correlations with mineralogical composition (Table 2) are established.

The first important correlation is found between particle size distribution (Fig. 5), mineralogical composition (Table 2) and Plasticity index

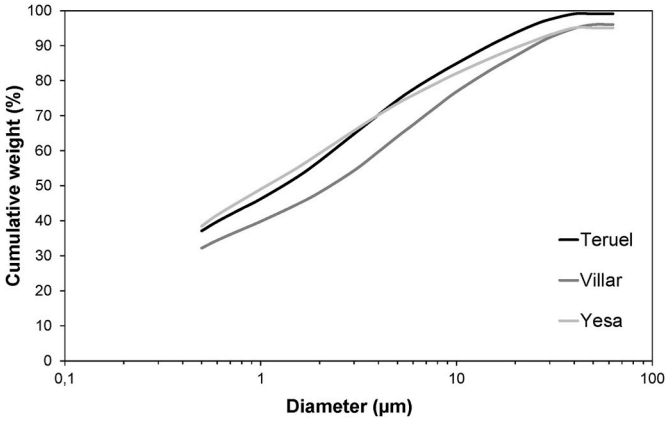

Fig. 5. Particle size distribution of the red firing clays used in this work after dry milling.

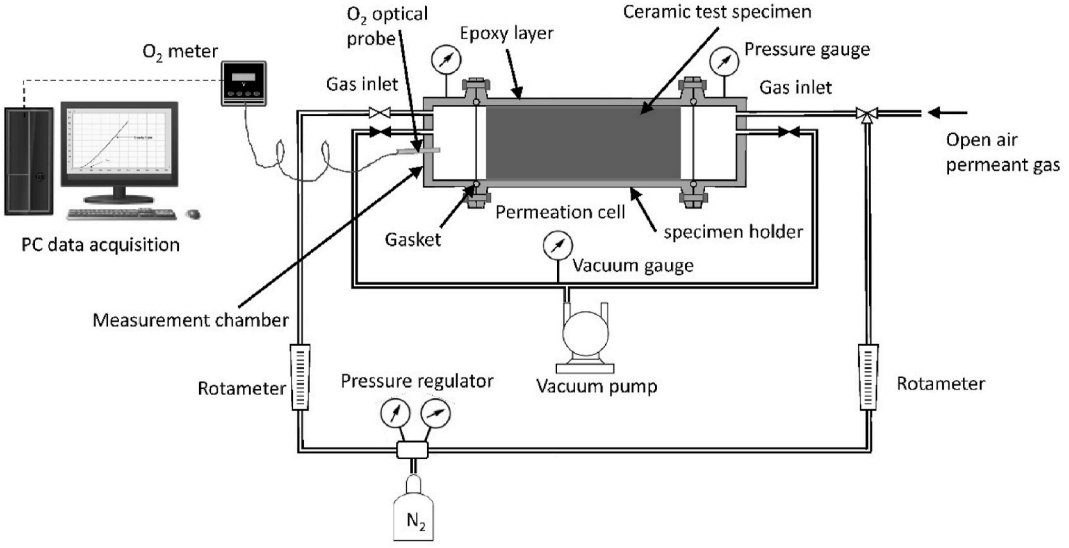

Fig. 4. Setup for the specimen Time lag tests.

Table 3
Plasticity, reject on a 63-μm sieve and extrusion behavior (water content, drying shrinkage and dry bulk density) of the red firing clays.

Clay	Teruel	Villar	Yesa
Plasticity Index (%)	28.0	24.0	31.5
Plastic limit (%)	19.5	18.5	21.0
63-μm Reject (%)	0.9	4.0	4.9
Water content (%)	20.3	19.3	22.2
Drying shrinkage (%)	6.1	5.9	6.9
Dry bulk density (g/cm^3)	2.05	2.11	2.08

(Table 3). Villar, the less plastic clay, has the lowest percentage of clayey minerals (kaolinite and illite) and its particle size distribution is characterized by the low percentage of small particles (below 2 μm). Yesa, on the contrary, has the highest percentage of small particles and it displays the highest plasticity. This is due to the higher percentage of clayey minerals (specially illite) with respect to Villar. Teruel has a somewhat different behavior which is due to the mainly kaolinitic character. According to the content of clayey minerals, higher than the rest of clays, Teruel should have the highest plasticity and the smallest particle size. However, as kaolinite (predominant in this clay) is usually characterized by particles which are coarser than those typical of illitic clays and therefore with lower specific surface, Teruel has an intermediate plasticity and its particle size distribution shows higher percentages of intermediate size but not so high percentages of fine particles. Plastic limit has been included in this table as the water content used in the extrusion process was closely related to that value. It can be seen that plastic limit has a good correlation with the index of plasticity, as typically clays with higher plasticity usually require higher water content to start developing a plastic behavior (which is the definition of plastic limit) [8–10].

The proportion of coarse particles, represented by the reject on a 63-μm sieve, also displays a close relationship with quartz content from the mineralogical analysis: Teruel, with the lowest quartz content, has the lowest reject on a 63-μm sieve.

The behavior in the shaping process has been evaluated by determining water content and drying shrinkage of extruded specimens (Table 3). Water content, as expected, increases with the plasticity of the clay (in fact, it is closer to plastic limit, PL, as the amount of water used in the kneading of each clay was fixed at LP+1%) and so does drying shrinkage, this last parameter showing a stronger increase. This is due to the fact that when plasticity increases, as it is the case of Yesa clay, not only there is an increase in water content (responsible of the drying shrinkage) but also there is a higher percentage of fine particles which usually tend to increase drying shrinkage in extruded specimens. In fact, chamotte, characterized by coarse particles, is commonly added to compositions processed by extrusion to reduce drying shrinkage.

Apart from the behavior in the shaping process, firing behavior is also very important as dimensional stability as well as a low pyroplastic deformation is required for the manufacturing of ceramic vessels. Vitrification diagrams of the three clays are plotted in Fig. 6 and Fig. 7. Each clay exhibits different fusibility, Teruel clay requiring the highest firing temperatures and Yesa clay the lowest. This different behavior can be explained with their mineralogical composition (Table 2). First of all, it must be taken into account that in red firing clays densification occurs by a liquid-phase sintering mechanism. Liquid-phase viscosity and its amount play a decisive role in this mechanism by establishing the rate at which the densification process occurs. Yesa clay, with the highest percentage of illite and the lowest of quartz, develops higher amount of liquid-phase than Villar clay. On the other hand, these two clays develop a liquid-phase which is rich in alkaline oxides, in contrast with Teruel clay, the most refractory clay due to its kaolinitic nature. Indeed, kaolinite provides a liquid-phase of higher viscosity because of the low proportion of alkaline oxides.

For the selection of optimum firing temperatures, open porosity of existing ceramic vessels has been taken into account, together with two restrictions: on the one hand it must not be so high so as to produce wine

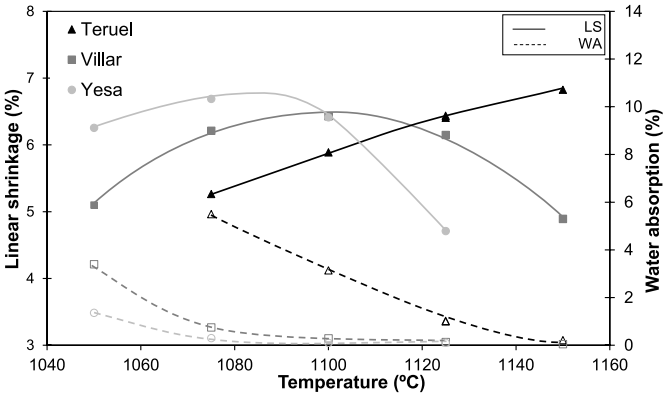

Fig. 6. Evolution of linear shrinkage and water absorption with firing temperature.

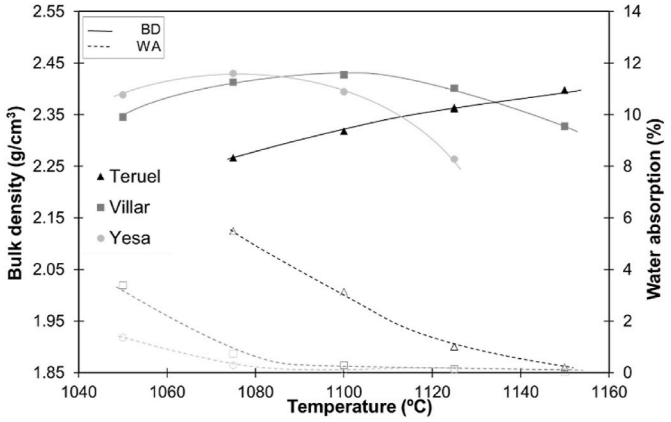

Fig. 7. Evolution of bulk density and water absorption with firing temperature.

leaking and therefore require sealing and on the other hand a certain porosity is needed to provide the microoxygenation required for wine maturation. By identifying the tendency to water permeation of the extruded specimens fired at different temperatures, a maximum value of open porosity was obtained. The test consisted of placing a glass cylinder on one of the sides of the piece filled with water and sealed to the surface of the piece (procedure used to determine chemical attack in standard EN-ISO 10545-13). In this case the cylinder with water remained for 24 h and water permeation in the opposite side was visually checked. Only the specimens with porosity higher than 8% led to water permeation, so maximum porosity has been fixed at this value, which also coincides with the maximum value available from the literature of existing ceramic vessels that do not require sealing (Table 1). The minimum value has been fixed at 2% considering the values of Table 1. Variation of open porosity as a function of firing temperature for the three clays is shown in Fig. 8, the maximum and minimum acceptable values shadowed in grey. From this figure optimum firing temperatures for each clay have been obtained.

Apart from a certain porosity, the main requirement for the use of a clay in the manufacturing of a vessel is its dimensional stability, this corresponding to both the absence of deformations in the vessel as well as to the homogeneity of dimensions among different vessels. This will only be achieved if firing shrinkage is not very high and presents a small variation with firing temperature, together with a low proneness to deform by pyroplasticity. In this way, typical gradients of temperature of the kilns and small variations of maximum temperature from one batch to another (considering intermittent firing) will not affect to the dimensions and therefore to the capacity of the vessel. In addition, a low deformation by pyroplasticity is also necessary to ensure dimensional

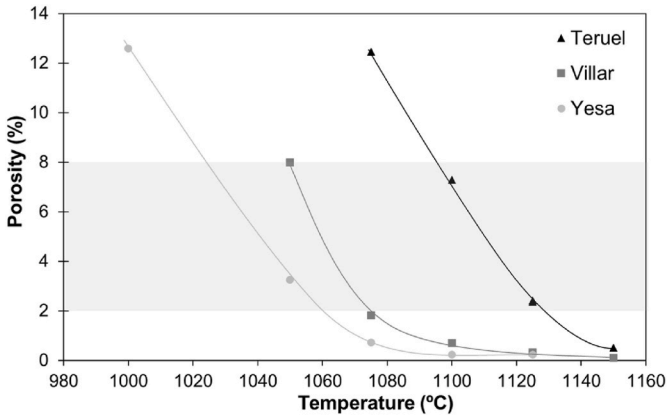

Fig. 8. Evolution of open porosity with firing temperature.

stability and specially a flat opening of the vessel, thus achieving a perfect sealing with the upper cover.

Regarding the values of linear shrinkage of the three clays and the variation with firing temperature (Fig. 6), all of them can be considered acceptable. Although there is no available data of shrinkage of the compositions used in the industrialized production of vessels such as those used in Clayver, Biopythos, etc., it is considered improbable a lower shrinkage with respect to the clays characterized in this work. And this is due to the high dry bulk density of the extruded specimens (and therefore, low porosity before firing), typical characteristic of these clays. White firing compositions such as those used in Clayver, Biopythos, etc. probably will not achieve such a high dry bulk density (ball clays typically provide significantly lower values of compacity due to the absence or lower proportion of coarse particles with respect to red firing Spanish clays used in ceramic tile production) and therefore it is deemed probable that firing shrinkage will be higher.

The other parameter already commented affecting dimensional stability, which is pyroplastic deformation, is strongly influenced by the type of clay, as it can be seen in Fig. 9. The trends observed among the three clays are those expected from their mineralogical composition, as it has been observed with all the properties previously discussed. Pyroplastic deformation strongly depends on liquid-phase viscosity [12, 13]. Therefore, Yesa clay, with the highest percentage of illite and the lowest of quartz, a liquid-phase richer in alkalis than Villar clay, with higher quartz content and lower of illite. And as was to be expected Teruel clay, with its kaolinitic nature, provides the liquid phase of higher viscosity and therefore, is the clay with the lowest tendency to deform by pyroplasticity. In addition, as was to be expected, for all the clays the index of pyroplasticity (*IP*) increases when firing temperature increases

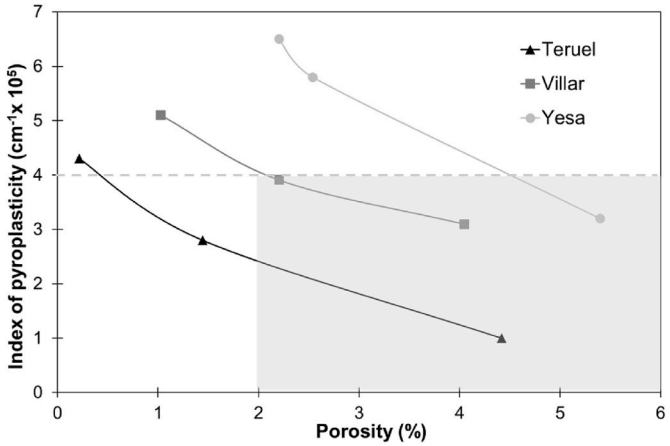

Fig. 9. Evolution of the index of pyroplasticity with open porosity.

(and porosity is reduced), as a consequence of the drop-in viscosity of the liquid-phase with increasing temperature.

It is important to note that values of the *IP* ranging from 2 to $5{\cdot}10^{-5}$ cm^{-1} are considered acceptable as they are common values of sintered ceramic materials such as stoneware tiles, porcelain tiles, sanitaryware and tableware. However, given the larger dimensions of the vessels with respect to these other ceramic products, a narrower interval (up to $4{\cdot}10^{-5}$ cm^{-1}, dashed line in Fig. 9) has been considered as the most adequate to ensure a sufficient dimensional stability. It is therefore clear that Teruel clay displays the best behavior, followed by Villar, which also provides acceptable values of the IP for porosities higher than 2% (being this the minimum porosity considered acceptable for a vessel as already explained). The greyish area of Fig. 9 shows the accepted interval of both *IP* and porosity, thus highlighting that in the case of Yesa clay only some of the values, those corresponding to porosities higher than 4.5%, are considered adequate.

From all these results, two firing conditions have been selected for each clay, one in the interval of low porosities (2–3%) and the other for high porosities (5–8%). These temperatures together with the values of bulk density, water absorption and open porosity are detailed in Table 4. The highest temperature selected for Yesa clay (with a low porosity) is out of the optimum interval already commented because it implies an unacceptable value of the index of pyroplasticity. It has been selected, however, to have a similar value of porosity for all the clays in order to be able to stablish the influence of pore size distribution (expected to vary from one clay to other) on the permeability and oxygen transmission rate without having the influence of porosity. These firing temperatures have been used to prepare specimens for the subsequent characterization performed in order to stablish the suitability of these clays for the manufacturing of vessels for wine fermentation and maturation in an industrialized framework.

3.2. *Pore size distribution*

According to the literature, pore volume and pore size distribution strongly influence permeability and therefore, oxygen transmission rate (*OTR*). Cumulative and differential pore size distributions are plotted in Figs. 10-14. In addition, Table 5 details, for the selected firing conditions, total pore volume and characteristic pore diameters of each clay. Porosity, determined from water absorption and bulk density, is also included. An overall look to these data reveals that as expected, characteristic pore diameters vary from one clay to another as well as with total porosity (that is, with firing temperature). Moreover, total pore volume, shows a high correlation with porosity. If the data are more carefully examined, both for the specimens with high porosity and for those with low porosity (Figs. 10 and 11 and Table 5), a relation between pore size, mineralogy and particle size can be observed. Villar and Yesa clays, with higher quartz content and higher residue on 63-μm sieve provide higher values of d_{16}, which corresponds to the coarser pores. The same thing happens with d_{50} although in minor extent as in this case probably the particles with intermediate size are the most influencing. On the other hand, the smallest pores, which are represented by the value of d_{84}, can be correlated with the content of clayey minerals (Table 2), thus being Teruel the clay with the lowest values of d_{84}. These differences of pore size can also be seen in the distributions, both in the

Table 4
Firing temperatures selected for each clay.

Sample	Temperature (°C)	Bulk density, BD (g/cm^3)	Water absorption, WA (%)	Porosity, ε (%)
Teruel	1100	2.34	3.1	7.2
	1125	2.39	1.0	2.4
Villar	1050	2.36	3.4	8.0
	1072	2.40	1.4	3.4
Yesa	1038	2.41	2.3	5.5
	1053	2.43	1.1	2.7

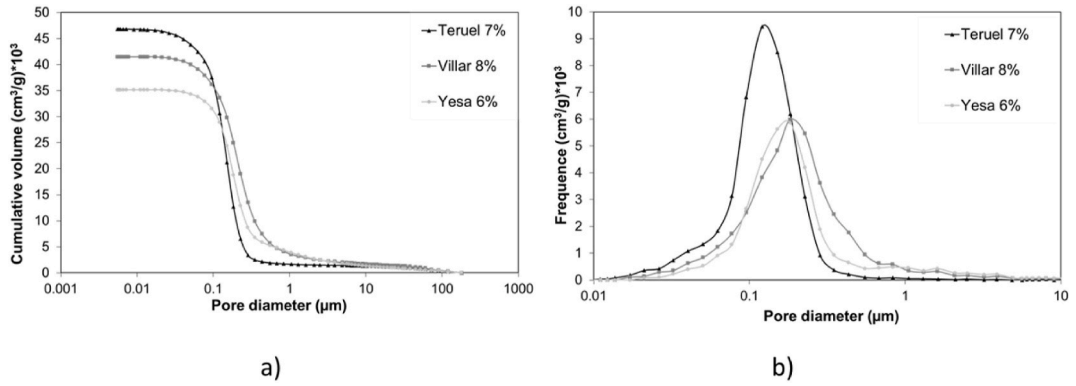

Fig. 10. Pore size distribution of the specimens with higher porosity obtained from the red firing clays: a) Cumulative volume and b) Frequency.

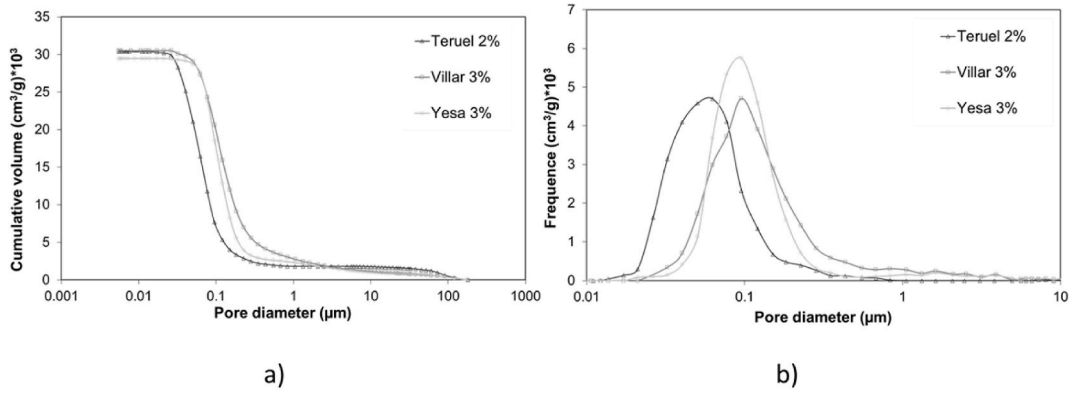

Fig. 11. Pore size distribution of the specimens with low porosity obtained from the red firing clays: a) Cumulative volume and b) Frequency.

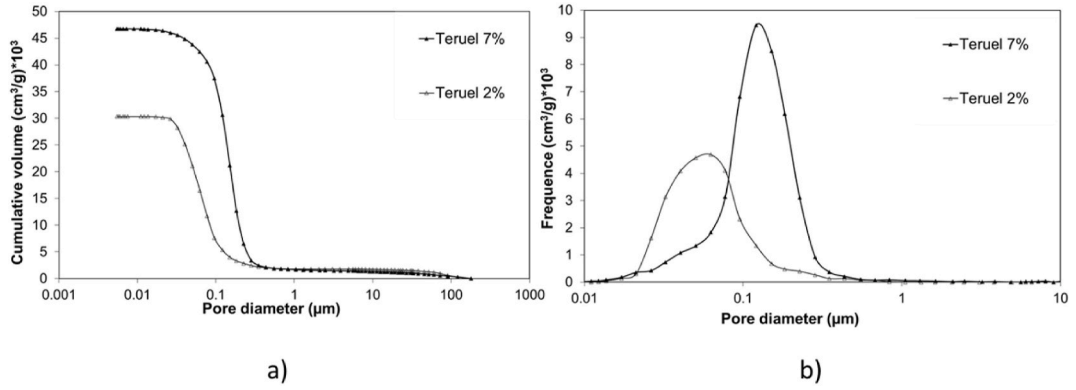

Fig. 12. Pore size distribution of the specimens obtained from Teruel clay: a) Cumulative volume and b) Frequency.

cumulated and in the differential, as Teruel clay has the distribution (in both porosities) displaced towards lower pore sizes. The three clays have been selected amongst those of high plasticity and finer particles so as to obtain small pores similar to those of existing vessels (Table 1, Clayver and Dolia). In this table the data of Dolia was obtained by the authors using the same process and equipment, and corresponds to the value of d_{50}. In the case of Clayver, the data was obtained from public data sheet 4,36]. In comparison with these data, the objective of providing similar pore sizes with respect to existing vessels has been achieved specially when compared to Dolia 5, although none of the three clays provide in the interval of porosities tested such a smaller pore size as Clayver (assuming that the value of 0.04 μm also corresponds to d_{50}, which is not indicated anywhere). More similar values of the three clays with respect to Dolia 5 than with respect to Clayver are logical because of the similar nature of the raw materials used in Dolia 5 (red firing clays from Andalucia, Spain) than those corresponding to Clayver (not published, but according to the white color probably composed of ball clays and non-plastic raw materials).

The preceding data are in good agreement, as already discussed, with the mineralogy of the clays. However, typically ceramic products show an increase in pore size when the sintering advances as the smallest pores are more easily closed under the action of liquid-phase and then, the coarsest pores become predominant while a reduction in total pore volume is observed [21]. In the three clays the behavior is the opposite, as it can be seen in Table 5 and in Figs. 12-14. When porosity decreases, the three clays are characterized as expected by a lower pore volume but also by a reduction in the proportion of the larger pores. Frequential pore size distributions clearly show that there is not a displacement

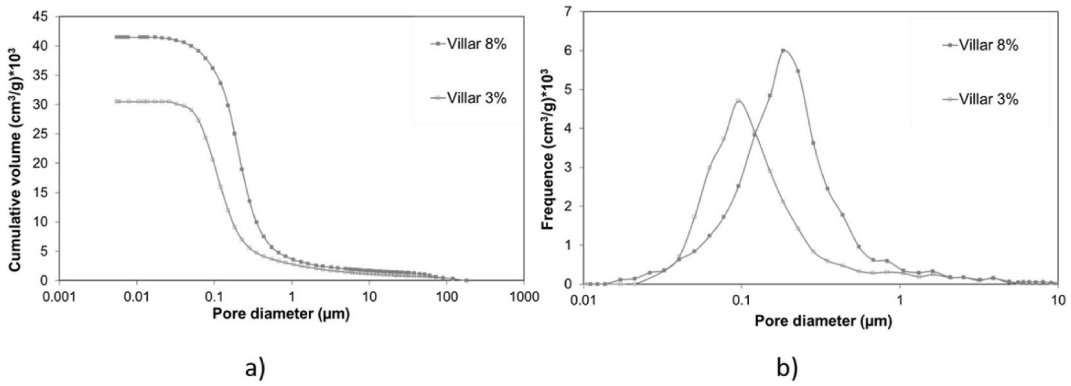

Fig. 13. Pore size distribution of the specimens obtained from Villar clay: a) Cumulative volume and b) Frequency.

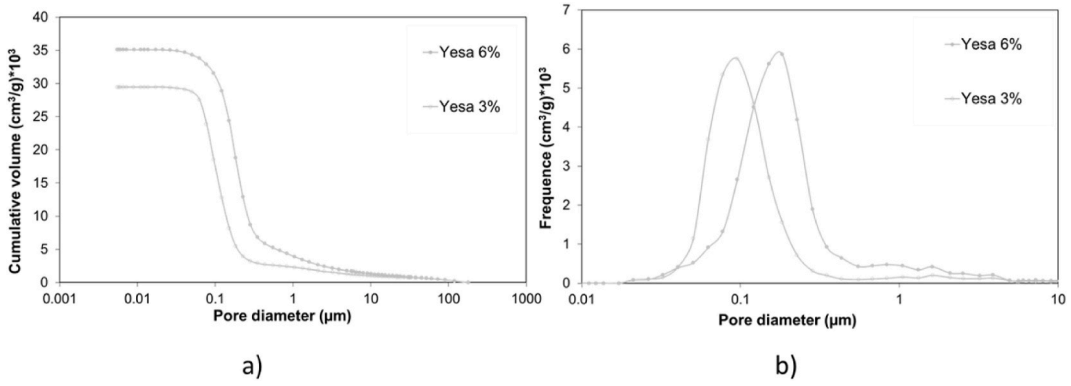

Fig. 14. Pore size distribution of the specimens obtained from Yesa clay: a) Cumulative volume and b) Frequency.

Table 5
Total pore volume and characteristic pore diameters together with firing temperature and porosity of the specimens obtained from the red firing clays.

Sample	Temperature (°C)	Porosity, ε (%)	d_{16} (μm)	d_{50} (μm)	d_{84} (μm)	Total pore volume (cm^3/g)
Teruel	1100	7.2	0.22	0.14	0.08	0.047
	1125	2.4	0.13	0.07	0.04	0.030
Villar	1050	8.0	0.49	0.21	0.11	0.042
	1072	3.4	0.34	0.13	0.07	0.031
Yesa	1038	5.5	0.48	0.19	0.11	0.035
	1053	2.7	0.20	0.11	0.07	0.030

towards smaller pores but a narrower distribution. This is due to the decrease in volume of the coarser pores, which apparently experience a reduction in size and therefore there is an increase in the volume of smaller pores. It is important to note that the behavior is common to the three clays, regardless of their mineralogy and firing temperatures required to reach similar porosities. This opposite behavior with respect to previous studies [21–24] must be due to a difference in microstructure as the literature found on the influence of sintering degree in pore size distributions usually is related to pressed specimens. In this case, dealing with extruded specimens with very low water content, the microstructure will probably differ significantly from that corresponding to pressed specimens.

In order to confirm the findings obtained in the determination of pore size distribution, the polished cross sections of the specimens

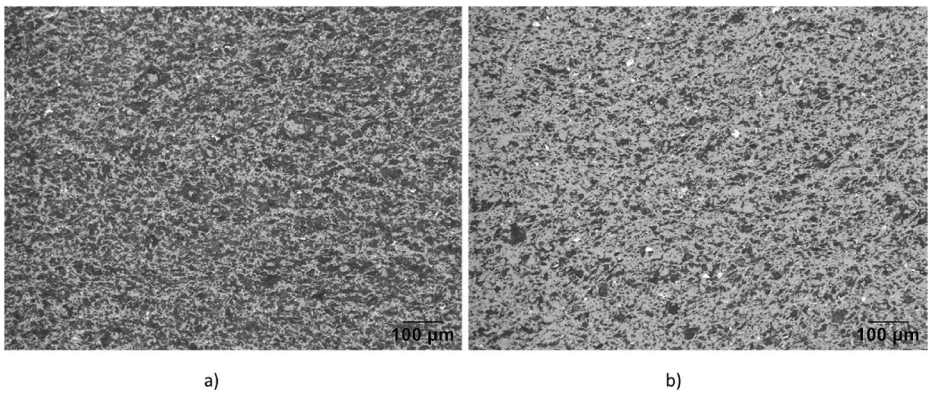

Fig. 15. Optical micrographs of the polished cross sections of specimens obtained from Teruel clay at the two sintering degrees a) open porosity 7% and b) open porosity 2%.

obtained from Teruel clay were examined in an optical microscope. Fig. 15 shows the two images obtained, in which a considerable change in porous texture is observed. Fig. 15 a) shows an interconnected porosity, typical of a not fully accomplished sintering degree and what is more important, with pores of larger size with respect to those obtained in the pore size distribution. Fig. 15 b) shows a considerable change, with a much denser microstructure in which the pores are becoming more isolated, but they are still of larger size with respect to those obtained in the pore size distribution. Although not coincident with pore size distributions, there is a common fact: when porosity decreases from 7% (a) to 2% (b), a reduction in pore size is observed, specially related to the coarser pores. The difference in pore size between the images of Fig. 15 and those obtained by Hg-porosimetry (Fig. 12) is due to the fact that the images of the optical microscope have been obtained from the cross sections of the extruded and fired specimens and show more realistically pore sizes. On the contrary, the pore size distributions determine the entering sections of each pore, which are usually of lower size than intermediate sections (Fig. 16) [23]. However, what is clear is that pore size distributions are the key results in order to analyze and correlate permeability and oxygen transmission rate with the characteristics of the specimens as gaseous flow through the exterior and interior surface of the ceramic vessels will depend more on the entering sections of the pores than in intermediate sections.

3.3. Determination of the permeation parameters

Table 6 details air permeability together with the oxygen permeation parameters for the two samples of different porosity of each clay. Average pore size (d_{50}) is also included. Oxygen Transmission Rate (*OTR*) is the most important parameter as it represents the flow of O_2 gas transported per unit of time through the surface of a specimen. *OTR* depends on oxygen permeability *P*, which in turn depends on the diffusion coefficient (diffusivity) *D*, and Henry's law solubility coefficient (solubility) *S*. A high *OTR* will lead to a fast maturation of the wine, since the processes of refining and color stabilization require the collaboration of oxygen. However, very high *OTRs* will not be acceptable because they can lead to a quick maturation of the wine, which is not desirable as it could impair its properties. On the other hand, very low *OTRs* are not acceptable too because it will increase the time required to finalize all the reactions in the wine. As each type of grape/wine can require a different degree of refining, the most suitable *OTRs* will depend on the type of grape and wine, this being a promising field of research for the future.

It is observed that for each clay the lower the porosity, the lower the air permeability and the oxygen permeation parameters: permeability, *OTR*, solubility and diffusivity, something already described in similar materials [1]. On the other hand, for similar porosities the type of clay also influences air permeability and the oxygen permeation parameters, with Teruel clay providing the lowest values of air and oxygen permeability and therefore of *OTR* and Villar clay the highest values, thus implying a strong influence of pore size on permeability and *OTR* as Teruel has the smallest pores and Villar the largest. It is clear, however, that porosity is much more influencing permeability and *OTR* than pore size, as the OTRs for the low porosity interval are much lower than the *OTRs* for the high porosity interval. A relation between permeability and *OTR* and pore size distribution is therefore envisaged, which has been successfully obtained in the next section (Discussion). In order to determine if the results obtained are adequate for the manufacturing of vessels for wine maturation, *OTR* values have been compared with those obtained with some specimens from Clayver [1], as they have been tested with the same procedure and equipment. These specimens, with varying porosities as a consequence of the different firing temperature, provided *OTR* values ranging from 294 to 613 $cm^3/m^2{\cdot}day$ (the higher the porosity, the higher the *OTR*). These values are higher than those obtained with the red firing clays in spite of the lower specimen thickness of the later (vessels manufactured with these clays would probably have higher thickness than the specimens tested (6–7 mm), to ensure mechanical strength and *OTR* will probably be reduced. Air permeability can also be a source of comparable data, as values from Dolia and from Clayver are available. The two types of Dolia provided air permeabilities of $250{\cdot}10^{-19}$ m^2 (Dolia 2, ceramic material with very high porosity, 16%) and $1–4{\cdot}10^{-19}$ m^2 (Dolia 5, ceramic material with porosity varying from 3 to 8% depending on the specific point of the vessel, a similar interval with respect to the red firing clays used in this work) and Clayver datasheet has a value of $46{\cdot}10^{-19}$ m^2. This last value, compared to those in Table 6, is in good agreement with the higher *OTR* of this type of ceramic material already discussed. The values of Dolia 5, on the other hand, are very similar to the values obtained with the red firing clays with low porosity.

It must be noted that real *OTR* values of vessels are obtained in wet conditions and strongly depend on specimen thickness, this type of test being used when all the parameters of industrial production of vessels are fixed. *OTR* values obtained in dry conditions (as those obtained in this work) are preferentially used to compare different materials and of course, there is a closed relationship between the two types of *OTR*.

Taking into account that both Dolia (in small scale production) and Clayver have been proved as successful materials for the manufacturing of vessels for wine maturation, the three clays provide acceptable values, although higher *OTRs* would be welcome. These higher OTRs can be obtained by reducing firing temperature or by using clays with coarser particle size distributions (for instance clays such as those from San Juan de Moró, Castellón, Spain and some types of Villar clay) [6].

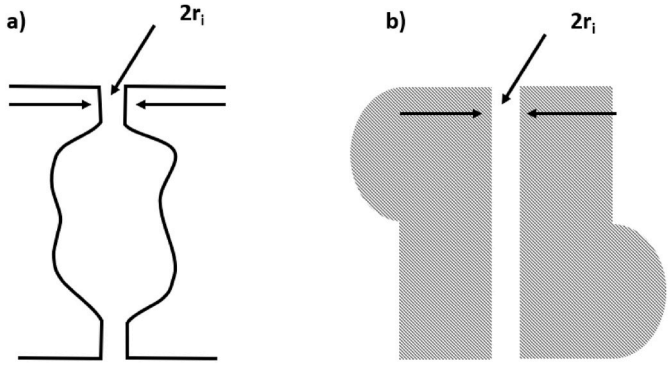

Fig. 16. Diagram of the error in determining the pore radius by mercury porosimetry, a) real pore and b) determined porous texture. Diagram from Ref. [23].

4. Discussion

In the present work, air permeability has been calculated based on Darcy's law [Eq. (10)], where $-dP/dx$ is the pressure gradient along the flow direction, μ is the absolute viscosity of the fluid, v_s is the superficial fluid velocity and k_1 is the Darcian permeability (expressed in dimensions of square length) [25].

$$-\frac{dP}{dx} = \frac{\mu}{k_1} v_s \tag{10}$$

For compressible fluids, as the air, the Eq. (10) is integrated, obtaining Eq. (2), used in the present work to calculate K_p. On the other hand, Ergun-related equations are used widely to predict fluid flow through porous media, modifying them depending on the porous media and the model developed. For instance, Das et al. [26] determined the average pore size using an Ergun-related equation, concluding that the pore diameters calculated from it were slightly higher than experimental results, as Ergun equation is based on beds of loose particles. Simão and coworkers [27] estimated the average fluid dynamic pore diameters of sintered bodies based on an Ergun-like relationship. Finally, Dey et al. [28,29] estimated the Darcian permeability constant k_1 theoretically by

Table 6
Porosity, ε; average pore size, d_{50}; air permeability, K_p; and oxygen permeation parameters: Oxygen Transmission Rate (*OTR*), diffusivity (D), permeability (P) and solubility coefficient (S).

Sample	ε (%)	d_{50} (μm)	$K_p \cdot 10^{19}$ (m^2)	OTR ($cm^3/m^2 \cdot day$)	$D \cdot 10^{10}$ (m^2/s)	$P \cdot 10^{17}$ ($m^3 \cdot m/m^2 \cdot s \cdot Pa$)	$S \cdot 10^{7}$ ($m^3/m^3 \cdot Pa$)
Teruel	7.2	0.14	6.2 ± 0.2 (4%)	133 ± 14 (10%)	3.2 ± 0.8 (25%)	10.3 ± 1.1 (10%)	3.4 ± 0.9 (27%)
	2.4	0.07	Out of range	41 ± 3 (8%)	1.8 ± 0.3 (15%)	3.1 ± 0.2 (8%)	1.8 ± 0.3 (15%)
Villar	8.0	0.21	15.0 ± 0.7 (5%)	169 ± 17 (10%)	4.5 ± 1.1 (24%)	15.8 ± 1.8 (11%)	3.7 ± 1.0 (26%)
	3.4	0.13	3.50 ± 0.15 (4%)	47 ± 5 (11%)	2.6 ± 0.7 (25%)	4.4 ± 0.5 (11%)	1.7 ± 0.5 (27%)
Yesa	5.5	0.19	7.3 ± 0.3 (4%)	130 ± 30 (23%)	4.9 ± 0.6 (12%)	14 ± 3 (23%)	2.9 ± 0.7 (23%)
	2.7	0.11	2.70 ± 0.13 (5%)	43 ± 6 (15%)	2.4 ± 0.4 (18%)	4.7 ± 0.7 (15%)	2.01 ± 0.4 (20%)

For permeation parameters: Mean ± SD; coefficient of variation in brackets.

means of Ergun-like equations and compared them with those obtained from experimentally measured data, concluding that Ergun equations work fine for k_1.

In the present work, the following Ergun-correlation [Eq. (11)], used to predict permeability of foams, has been used to correlate the air permeability to the properties of the ceramic specimen (porosity and mean pore size), taking the equivalent pore size as the mean pore size obtained in the mercury porosimetry:

$$k_1 = \frac{\varepsilon^2 d_C^2}{36\tau(\tau - 1)} \tag{11}$$

Where τ is the tortuosity of the porous matrix, ε is the porosity and d_C is an equivalent pore size [25]. The results have been depicted in Fig. 17, where it can be seen that there is a lineal relationship between the air permeability constant and the porosity and pore size ($\varepsilon^2 \cdot d_{50}^2$); furthermore, data obtained from previous studies with Dolia samples [30] with similar porosity values have been added. It can be seen that experimental data of air permeability and the product ($\varepsilon^2 \cdot d_{50}^2$) follows a linear relationship; moreover, data from Dolia sample seem to follow also a linear tendency. Consequently, due to the good result obtained in the lineal adjustment of the experimental data, it is possible to assume that values of tortuosity are similar for the different specimens, possibly because the same forming method has been used (extrusion). The differences between Dolia's results and the actual results can be related with the different forming method of both samples, since Dolia samples were obtained from vessels (formed with a roller equipment). It has thus been shown that this is an appropriate model to evaluate how air permeability changes when the main properties of the sample's microstructure change and to predict air permeability in samples of the same origin and different characteristics.

In the following figures, data obtained from Darcy's law (air permeability, K_p) and from Fick's law (Oxygen Transmission Rate, *OTR*, in Fig. 18 and the oxygen permeation coefficient, *P*, in Fig. 19) have been compared. In both figures, SD of data of each specimen has been depicted (error bars). As it can be seen, both parameters obtained from Fick's law (*OTR* and *P*) and K_p can be adjusted with a logarithmic relationship. As in the previous figure, although these relationships cannot be used as general equations (they depend on the nature, dimensions, etc. of each specimen), it is a good approximation to evaluate the dependence of the different parameters and to predict the variation of *OTR* and *P* when the characteristics of the ceramic samples are changed (porosity, mean pore size and, consequently, air permeability). This can be very useful to design composition and to modify process' parameters in the manufacture of ceramic vessels with different values of *OTR*.

Moreover, given the relationship between pore size distribution and the characteristics of the clays introduced in section 3.2 and the relations obtained between *OTR* and air permeability on the one hand and between air permeability and porosity and pore size on the other hand, a further correlation (Fig. 20) has been found between particle size distribution of the clay (more precisely, the percentage of small particles i.e. below 0.5 μm) and the *OTR* for the specimens with high porosity and therefore high *OTR*. This correlation is considered reasonable because the percentage of small particles i.e. below 0.5 μm is related to the clayey minerals, as already discussed, which are those influencing porous microstructure of the unfired pieces and then, of the pieces corresponding to the early sintering stages.

For the low porosity interval this correlation is not satisfactory,

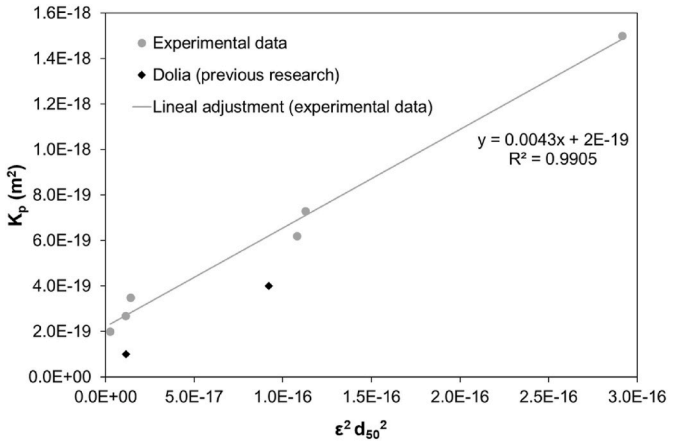

Fig. 17. Relation between air permeability, K_p, and ($\varepsilon^2 \cdot d_{50}^2$) (ε: porosity, d_{50}: mean pore size). Note: K_p value of sample "Teruel 2.4% porosity" was out of range, so, to analyze this relation, the selected value of K_p is the minimum that the air permeability device (Fig. 2) can measure ($2 \cdot 10^{-19}$ m^2).

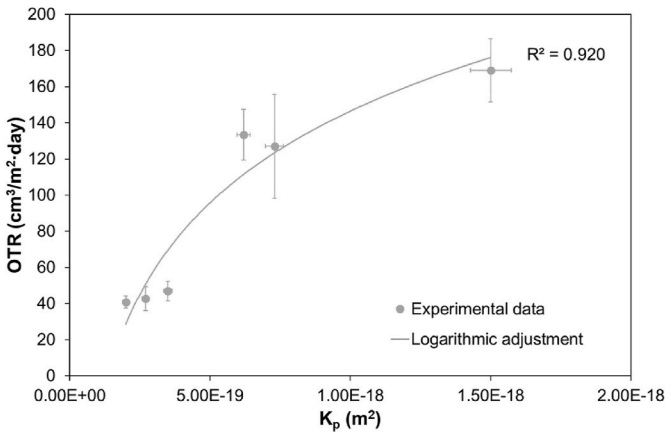

Fig. 18. Relationship between Oxygen Transmission Rate (OTR) and air permeability (K_p).

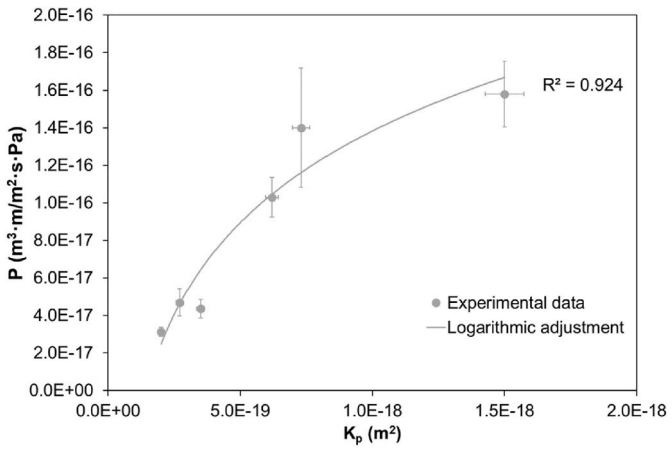

Fig. 19. Relationship between oxygen permeation coefficient (P) and air permeability (K_p).

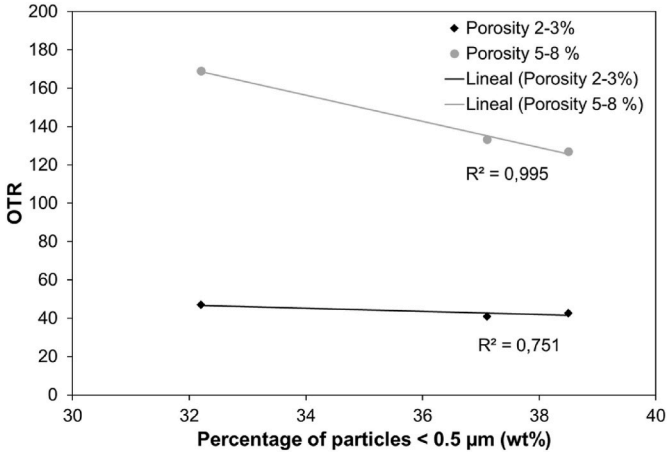

Fig. 20. Relationship between Oxygen Transmission Rate (OTR) and percentage of particles <0.5 μm of the clay.

especially because very low *OTRs* and a very low variation between the three clays have been obtained (*OTRs* ranging from 41 to 47 cm^3/m^2•day in this interval while *OTRs* for the high porosity interval lie within the range 130–169 cm^3/m^2•day). In addition, the low porosity interval corresponds to a high sintering degree in the presence of vitreous phase in which pore size change with respect to the high porosity interval for the three clays studied (Table 5 and Figs. 12-14). So, it is considered reasonable that the correlation between particle size and *OTR* is found for earlier stages of the sintering process rather than for advanced sintering in the presence of high amounts of vitreous phase.

As already discussed, higher *OTRs* can be obtained by reducing firing temperature or by using clays with coarser particle size distributions (for instance clays such as those from San Juan de Moró, Castellón, Spain and some types of Villar clay [6], also belonging to the same orographic system than the three clays under study). It is deemed more likely to use clays with coarser particle size distributions than to reduce firing temperature because this last could lead to wine permeation because of the higher porosity implied. Moró clay and low plasticity clays from Villar could be used to increase pore size without changing appreciably porosity and therefore, to obtain higher permeabilities and *OTRs*. This is due to their coarser particle sizes, as it can be seen in Table 7, that, as previously confirmed, will lead to higher pore sizes. In fact, the equation obtained to correlate *OTR* with the percentage of particles below 0.5 μm of Fig. 20 has been used to predict (of course with a considerable uncertainty due to the extrapolation in particle size) which *OTRs* could be achieved with these alternative clays when fired at the temperatures required to obtain high porosities (5–8%). The values obtained are 252 for Low Plasticity Villar and 306 for Moró, which are much closer to the data corresponding to Clayver (294–613 cm^3/m^2•day).

Table 7
Reject on a 63-μm sieve, percentage of particles below 10 μm and percentage of particles below 0.5 μm of the three red firing clays characterized in this work and red firing clays potentially useful to increase pore sizes.

Sample	Reject on a 63-μm sieve	Percentage of particles below 10 μm (wt%)	Percentage of particles below 0.5 μm (wt%)
Teruel	0.9	84.9	37.1
Villar	4.0	76.8	32.2
Yesa	4.9	82.1	38.5
Low plasticity Villar [5]	10	67	20
Moró [6]	31	56	12

5. Conclusions

By selecting three red firing clays with different chemical and mineralogical composition and particle size distribution, correlations have been obtained between these characteristics and plasticity and process behavior (extrusion and firing stages). Parameters such as water content in the plastic mass and drying shrinkage show, as expected, a close relationship with the plasticity, particle size distribution and mineralogical composition of the clay. Yesa clay, with a high content of illite and the highest plasticity index requires the highest water content in the extrusion process and has the highest drying shrinkage. Villar, on the contrary, due to its high quartz content and lower content of clayey minerals requires the lowest water content in the extrusion process and has the lowest drying shrinkage. Optimum firing temperatures and the index of pyroplasticity, IP, also depend strongly on clay mineralogy, being Teruel the most refractory clay with the lowest IP due to its kaolinitic nature.

Regarding their suitability of use from a wine maker perspective, particle size distribution (PSD) of the clay has been proved to be the most influencing parameter (apart from porosity, that can be modified by varying firing temperature) on oxygen transmission rate (*OTR*). This is due to the influence of PSD on pore size distribution of the fired specimens and to the relationship stablished in this work between porosity and pore size and air permeability and to the correlations between air permeability and *OTR* and between PSD (percentage of particles below 0.5 μm) and *OTR* for the high porosity interval. From these results, the three clays have been proved as suitable for the manufacture of ceramic vessels because of their adequate behavior in the manufacturing process (although in the case of Yesa clay only medium-high porosities can be achieved in order not to compromise dimensional stability) and similar permeability with respect to certain types of existing ceramic vessels. Compared to the data of *OTR* of existing vessels (Clayver type), the values obtained are lower but with the same order of magnitude, and other clays from the same region have been postulated as the key for achieving higher *OTRs*.

Declaration of interests

The authors declare that they have no known competing financial interests or personal relationships that could have appeared to influence the work reported in this paper.

Acknowledgements

This project has been supported by the European Union through the European Agricultural Fund for Rural Development (FEADER) and the Ministry of Agriculture, Fisheries and Food (MAPA), under the National Rural Development Program 2014–2020. It has also been co-funded by

the Instituto Valenciano de Competitividad Empresarial (IVACE) of the Valencian Region Government (GVA).

References

[1] I. Nevares, M. Del Alamo-Sanza, Characterization of the oxygen transmission rate of new-ancient natural materials for wine maturation containers, Foods 10 (2021) 1–27, https://doi.org/10.3390/foods10010140.

[2] A.J. Polvorinos Del Río, V. Flores, M.A. Tabales, M.J. Hernández, Caracterización y tecnología de materiales cerámicos romanos de los ss. I a III d.c procedentes del Hospital de las Cinco Llagas de Sevilla, Bol. La Soc. Española Ceram. y Vidr. 42 (2003) 93–99, https://doi.org/10.3989/cyv.2003.v42.i2.647.

[3] J.F. Shackelford, P.L. Shackelford, Ceramics in the wine industry, Int. J. Ceram. Eng. Sci. 3 (2021) 18–20, https://doi.org/10.1002/ces2.10073.

[4] J. Banegas, El hormigón y las tinajas como envases en la elaboración y maduración de vinos, in: F. para la cultura del Vino (Ed.), Gestión Del Oxígeno y Elabor. y Envejec. En Envases Altern. XII Encuentro Técnico, Madrid, Spain, 2017, pp. 97–109. https://www.culturadelvino.org/fcv/wp-content/uploads/pdf/encuentros/encuentro_2018.pdf.

[5] A. Barba, V. Beltrán, C. Feliu, J. García-Ten, F. Ginés, E. Sánchez, V. Sanz, Materias primas para la fabricación de soportes de baldosas cerámicas, second ed., Instituto de Tecnología Cerámica, Castellón, 2000.

[6] V. Beltrán, V. Bagan, E. Sánchez, F. Negre, Características técnicas de las arcillas utilizadas para la fabricación de pavimentos y revestimientos cerámicos en pasta roja, Tec. Cerámica. (1988) 280–287.

[7] R. Alegre Molina, Arcillas caoliníferas y materiales asociados de la facies Weald (Formación Camarillas) de la provincia de Teruel: Caracterización mineral y génesis, Trabajo de Fin de Grado, Universidad de Zaragoza, Facultad de Ciencias, 2015.

[8] F. Ginés, C. Feliu, J. García-Ten, V. Sanz, Análisis de los métodos tradicionales utilizados para evaluar la plasticidad, Bol. La Soc. Española Ceram. y Vidr. 36 (1997) 25–30.

[9] V. Doménech, E. Sánchez, V. Sanz, J. García, F. Ginés, Estimacion de la plasticidad de masas ceramicas mediante la determinacion de la fuerza de indentacion, Qualicer, 1994, pp. 61–71.

[10] V. Doménech, J. García-Ten, F. Ginés, E. Sánchez, V. Sanz, Estimación de la plasticidad de masas cerámicas mediante la determinación de la fuerza de indentación, Cerámica Inf. (1994) 7–15.

[11] J.L. Amorós, V. Beltrán, A. Blasco, C. Feliu, M. Sancho-Tello, Técnicas experimentales del control de la compactación de pavimentos y revestimientos cerámicos, Técnica Cerámica 116 (1983) 1234–1246.

[12] J. García-Ten, M. Quereda, A. Saburit, Influencia del Talco CV 3 Piedra sobre el comportamiento y propiedades del Gres Porcelánico Técnico. Parte 1: composiciones Base, Técnica Cerámica 294 (2001) 737–747.

[13] A. Escardino, Amo, C. Feliu, F. Negre, Defectos de planaridad en las piezas de pavimento gresificado motivados por deformación piroplástica. Influencia de las variables de proceso, Taulells 3 (1985) 3–9.

[14] K. Müller, Z. Scheuerer, V. Florian, T. Skutschik, S. Sängerlaub, Comparison of test methods for oxygen permeability: optical method versus carrier gas method, Polym. Test. 63 (2017) 126–132, https://doi.org/10.1016/J.POLYMERTESTING.2017.08.006.

[15] M. Lomax, Permeation of gases and vapours through polymer films and thin sheet-part I, Polym. Test. 1 (1980) 105–147, https://doi.org/10.1016/0142-9418(80)90037-9.

[16] M.G. De Angelis, Solubility coefficient (S), in: Encycl. Membr., Berlin Heidelberg, Springer, 2014, pp. 1–5.

[17] H. Larsen, A. Kohler, E.M. Magnus, Ambient oxygen ingress rate method—an alternative method to Ox-Tran for measuring oxygen transmission rate of whole packages, Packag. Technol. Sci. 13 (2000) 233–241, https://doi.org/10.1002/pts.519.

[18] I. Nevares, M. Del Alamo-Sanza, New materials for the aging of wines and beverages: evaluation and comparison, Food Packag. Preserv. (2018) 375–407.

[19] M.R. Shah, R.D. Noble, D.E. Clough, Measurement of sorption and diffusion in nonporous membranes by transient permeation experiments, J. Membr. Sci. 287 (2007) 111–118, https://doi.org/10.1016/j.memsci.2006.10.026.

[20] J.-B. Diéval, S. Vidal, O. Aagaard, Measurement of the oxygen transmission rate of Co-extruded wine bottle closures using a luminescence-based technique, Packag. Technol. Sci. 24 (2011) 375–385, https://doi.org/10.1002/pts.945.

[21] M.J. Orts, A. Escardino, J.L. Amorós, F. Negre, Microstructural changes during the firing of stoneware floor tiles, Appl. Clay Sci. 8 (1993) 193–205.

[22] J.L. Amorós, V. Beltrán, A. Escardino, M.J. Orts, Permeabilidad al aire de soportes cocidos de pavimento cerámico. I. Influencia de las variables de prensado y de la temperatura de cocción, Boletín La Soc. Española Cerámica y Vidr. 31 (1992) 33–38.

[23] J.L. Amorós, V. Beltrán, A. Escardino, M.J. Orts, Permeabilidad al aire de soportes cocidos de pavimento cerámico. II. Relación entre el coeficiente de permeabilidad al aire y las propiedades características de la estructura porosa del sólido, Boletín La Soc. Española Cerámica y Vidr. 31 (1992) 207–212.

[24] J. García-Ten, M.J. Orts, A. Saburit, G. Silva, Thermal conductivity of traditional ceramics. Part 1: influence of bulk density and firing temperature, Ceram. Int. 36 (2010) 1951–1959.

[25] M.D. de Mello Innocentini, P. Sepulveda, F. dos Santos Ortega, C. Scheffler, M. Paolo, Permeability, in: M. Scheffler, P. Colombo (Eds.), Cell. Ceram. Struct. Manuf. Prop. Appl., Wiley-VCH; John Wiley [distributor], Weinheim; Chichester, 2005, pp. 313–341.

[26] D. Das, N. Kayal, G.A. Marsola, L.A. Damasceno, M.D.D.M. Innocentini, Permeability behavior of silicon carbide-based membrane and performance study for oily wastewater treatment, Int. J. Appl. Ceram. Technol. 17 (2020) 893–906, https://doi.org/10.1111/ijac.13463.

[27] L. Simão, R.F. Caldato, M.D.M. Innocentini, O.R.K. Montedo, Permeability of porous ceramic based on calcium carbonate as pore generating agent, Ceram. Int. 41 (2015) 4782–4788, https://doi.org/10.1016/j.ceramint.2014.12.031.

[28] A. Dey, N. Kayal, O. Chakrabarti, R.F. Caldato, C.M. André, M.D.M. Innocentini, Permeability and nanoparticle filtration assessment of cordierite-bonded porous sic ceramics, Ind. Eng. Chem. Res. 52 (2013) 18362–18372, https://doi.org/10.1021/ie402876v.

[29] A. Dey, N. Kayal, O. Chakrabarti, M.D.M. Innocentini, W.S. Chacon, J.R. Coury, Evaluation of air permeation behavior of porous SiC ceramics synthesized by oxidation-bonding technique, Int. J. Appl. Ceram. Technol. 10 (2013) 1023–1033, https://doi.org/10.1111/j.1744-7402.2012.02847.x.

[30] M. Quereda, M.-M. Lorente-Ayza, P. Escrig, M. Ojeda, Tinajas cerámicas para la maduración del vino: de la fabricación artesanal al proceso tecnológico, in: LVII Congr. Nac. La Soc. Española Cerámica y Vidr., Castelló de la Plana, 2020, p. IO07008.

Web references

31 http://www.tinajasorozco.com/.

32 https://tinajasmorenoleon.com/.

33 https://www.oeno-tech.ch/.

34 https://www.tava.it/.

35 https://biopythos.fr/.

36 https://www.clayver.it/en/.

37 https://www.vitisphere.com/news-94097-maturing-wines-in-amphorae-produced-with-a-3-d-printer.html.